

We are IntechOpen, the world's leading publisher of Open Access books Built by scientists, for scientists

6,900

Open access books available

185,000

International authors and editors

200M

Downloads

Our authors are among the

154

Countries delivered to

TOP 1%

most cited scientists

12.2%

Contributors from top 500 universities



WEB OF SCIENCE™

Selection of our books indexed in the Book Citation Index
in Web of Science™ Core Collection (BKCI)

Interested in publishing with us?
Contact book.department@intechopen.com

Numbers displayed above are based on latest data collected.
For more information visit www.intechopen.com



Power Balance Mode Control for Boost-Type DC-DC Converter

Taichi Kawakami

Abstract

In recent years, the demand for switching converters has steadily increased. The desired converters need to be small and have high power density, good efficiency, good responsiveness, and good robustness. High responsiveness and high robustness are required for the control systems of switching converters. Some studies suggest that responsiveness and robustness can be improved using current mode control. However, it is difficult to improve the control performance of boost-type DC-DC converters significantly only by using these technologies. The power balance mode control approach can be used for solving various problems. In this approach, control is exerted to eliminate the difference between the input power and the output power. As a result, responsiveness and robustness can be improved when compared to the conventional control method. In this study, the effectiveness of the power balance mode control is confirmed using a circuit simulator.

Keywords: boost-type DC-DC converter, voltage mode control (VMC), current mode control (CMC), sliding mode control (SMC), digital control, responsiveness, robustness

1. Introduction

The demand for switching converters has been steadily increasing. The desired converters should be small and have high power density, high efficiency, good responsiveness, and good robustness. High responsiveness and high robustness are required for the control systems of switching converters. Voltage mode control (VMC) is the most basic control system of switching converters [1, 2]. Since the voltage mode control uses only one voltage sensor, it can be constructed at very low cost. However, since the stability of the control system is low, current mode control (CMC) is used for a general switching converter [3, 4]. Some studies suggest that responsiveness and robustness can be significantly improved using the current mode control (CMC) approach [1–4]. However, it is difficult to improve the performance of boost-type DC-DC converters significantly using only this technology. Although buck-type DC-DC converters can be regarded as approximately linear circuits (regardless of the time-varying circuit), this is not so for boost-type DC-DC converters. This is because in boost-type DC-DC converters, the ON and OFF circuit states are different. As a result, the transfer function of any boost-type DC-DC converter includes an unstable zero (right half plane zero (*RHP-zero*)). Therefore, control systems based on boost-type DC-DC converters cannot set the

gain-crossover frequency (which determines the high-frequency response) due to the presence of this unstable zero.

On the other hand, control of switching converter using sliding mode control (SMC) has been studied [5–9]. Sliding mode control has high robustness and is resistant to influences by plant fluctuations. However, the control system has a problem that it is very complicated compared with VMC and CMC.

In this research, we developed power balance mode control (PBMC), which is a new control method that incorporates SMC concept into CMC [10]. In the PBMC approach, the input voltage and the output current are incorporated into the control system as in the conventional control method, and new control items are added by calculation. As a result, the performance of the control system can be greatly improved, when compared with the conventional control method. Furthermore, since the added control items are constituted by four arithmetic operations, implementation is also very easy.

2. Transfer functions of the boost-type DC-DC converter

In this study, a single-phase boost-type DC-DC converter was used as a plant. **Figure 1** shows the circuit diagram of the plant. To obtain the transfer function of this plant, a modeling method called the state-space averaging method was used. In this section, various transfer functions used for designing the control system of the DC-DC converter are described.

2.1 Derivation of the transfer function model using the state-space averaging method

The switching converter is a time-varying circuit in which the state of the circuit can be set to either ON or OFF. Therefore, the state-space averaging method [11–13], which averages the circuit by a duty ratio, was used. The derivation for obtaining the transfer function of the switching converter using the state-space averaging method is shown below.

2.1.1 Circuit state ($Q_1 = \text{ON/OFF}$) and state space equation

For circuit averaging, it is necessary to determine the circuit's ON/OFF states. When mathematically modeling the state of a circuit, the state equation and the following output equation are used:

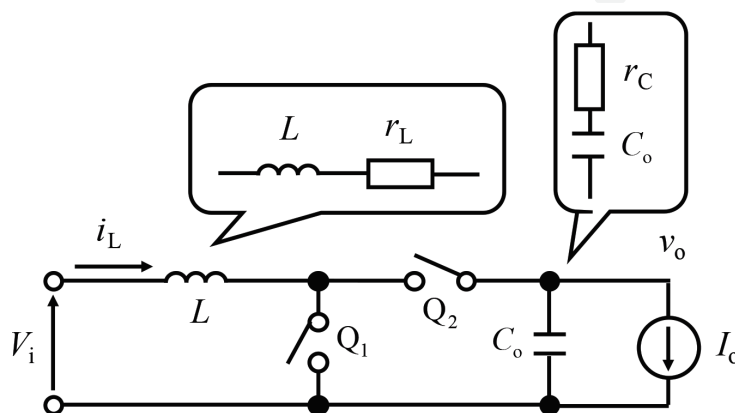


Figure 1.
Single-phase boost-type DC-DC converter.

$$\begin{cases} \frac{d\mathbf{x}(t)}{dt} = \mathbf{A}\mathbf{x}(t) + \mathbf{b}u(t) \\ y(t) = \mathbf{c}\mathbf{x}(t) + \mathbf{d}u(t) \end{cases} \quad (1)$$

where $\mathbf{u}(t)$, input vector; $\mathbf{x}(t)$, state vector; $y(t)$, output vector; \mathbf{A} , state matrix; \mathbf{b} , input matrix; \mathbf{c} , output matrix; \mathbf{d} , direct matrix.

With respect to the circuit shown in **Figure 2**, the state equation and the output equation are expressed using the following equations:

$$\begin{cases} \frac{d}{dt} \begin{bmatrix} i_L(t) \\ v_C(t) \end{bmatrix} = \begin{bmatrix} a_{11} & a_{12} \\ a_{21} & a_{22} \end{bmatrix} \begin{bmatrix} i_L(t) \\ v_C(t) \end{bmatrix} + \begin{bmatrix} b_{11} & b_{12} \\ b_{21} & b_{22} \end{bmatrix} \begin{bmatrix} V_i(t) \\ I_o(t) \end{bmatrix} \\ v_o(t) = [c_{11} \ c_{12}] \begin{bmatrix} i_L(t) \\ v_C(t) \end{bmatrix} + [d_{11} \ d_{12}] \begin{bmatrix} V_i(t) \\ I_o(t) \end{bmatrix} \end{cases} \quad (2)$$

In Eq. (2), the inductor current and capacitor voltage comprise the state vector, while the input voltage and the output current comprise the input vector. **Figure 2** shows the equivalent circuit for the ON and OFF states of the switch Q_1 .

2.1.2 Circuit state averaging using duty ratio

When the state of a circuit is averaged over one switching period using the duty ratio, the state equation and the output equation are given as follows:

$$\begin{cases} \frac{d\bar{\mathbf{x}}(t)}{dt} = (D\mathbf{A}_{\text{on}} + D'\mathbf{A}_{\text{off}}) \cdot \bar{\mathbf{x}}(t) + (D\mathbf{b}_{\text{on}} + D'\mathbf{b}_{\text{off}}) \cdot \bar{\mathbf{u}}(t) \\ \bar{v}_o(t) = (D\mathbf{c}_{\text{on}} + D'\mathbf{c}_{\text{off}}) \cdot \bar{\mathbf{x}}(t) + (D\mathbf{d}_{\text{on}} + D'\mathbf{d}_{\text{off}}) \cdot \bar{\mathbf{u}}(t) \\ D' = 1 - D \end{cases} \quad (3)$$

Here D and D' represent the time ratio of the ON and OFF periods in one switching cycle, respectively. The switching converter averages the circuit state by the duty ratio, and it can be regarded as a linear time-invariant system for frequencies lower than the switching frequency. Additional characterization includes static characteristic analysis, steady-state dynamic analysis, and Laplace transforms. Although the transfer function of the switching converter can be derived using the above, in this study the following derivation is omitted. The transfer function of the

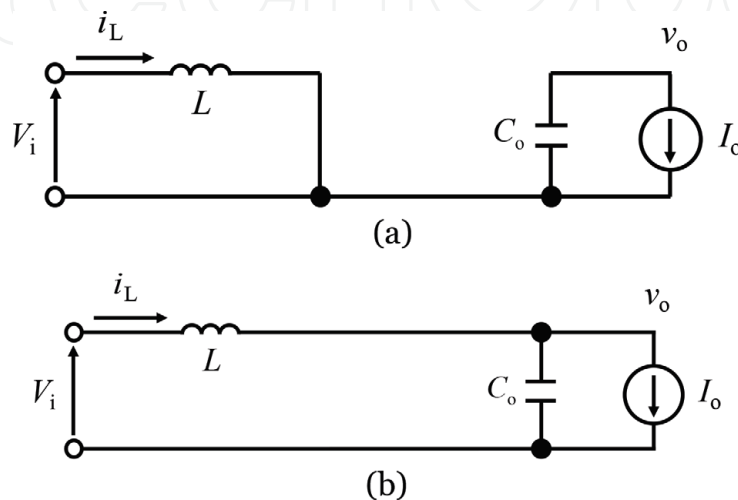


Figure 2.
 Equivalent circuits for the ON and OFF states. (a) Switch Q_1 : ON; (b) switch Q_1 : OFF.

single-phase boost-type DC-DC converter is shown in Eq. (4). The transfer functions derived using the state-space averaging method include output impedance and audio susceptibility. In this chapter, the most important transfer function is described in the control system design of the switching converter.

$$\left\{ \begin{array}{l} G_{id}(s) = \frac{\Delta I_L(s)}{\Delta D(s)} = \frac{K_{dc_i}}{P(s)} \left(1 + \frac{s}{\omega_o} \right) \\ G_{vd}(s) = \frac{\Delta V_o(s)}{\Delta D(s)} = \frac{K_{dc_v}}{P(s)} \left(1 + \frac{s}{\omega_{esr}} \right) \left(1 - \frac{s}{\omega_{rhp}} \right) \\ K_{dc_i} = \frac{I_o}{D'^2} \quad K_{dc_v} = \frac{V_i}{D'^2} \\ \frac{1}{P(s)} = \frac{\omega_n^2}{s^2 + 2\zeta\omega_n s + \omega_n^2} = \frac{1}{\left(\frac{s}{\omega_n}\right)^2 + \frac{2\zeta}{\omega_n}s + 1} \\ \zeta = \frac{r_L + D'r_C}{2D'} \sqrt{\frac{C_o}{L}} \\ \omega_n = \frac{D'}{\sqrt{LC_o}} \quad \omega_o = \frac{I_o}{C_o V_o} \quad \omega_{esr} = \frac{1}{C_o r_C} \quad \omega_{rhp} = \frac{D'V_i}{LI_o} \end{array} \right. \quad (4)$$

where $G_{id}(s)$, transfer function of the duty ratio to the inductor current; $G_{vd}(s)$, transfer function of the duty ratio to the output voltage; K_{dc_i} , DC gain of $G_{id}(s)$; K_{dc_v} , DC gain of $G_{vd}(s)$; $1/P(s)$, second-order lag system; ζ , damping factor; ω_n , resonance frequency; ω_o , zero frequency of load of the boost-type DC-DC converter; ω_{esr} , ESR zero frequency of the output smoothing capacitor; ω_{rhp} , right half plane (RHP) zero frequency.

2.2 Pulse modulation gain: F_m

Because the switching converter is controlled by the pulse width modulation (PWM) signal corresponding to the duty ratio, it is necessary to modulate the control signal from the compensator to the PWM signal. **Figure 3** shows the correspondence between the control signal and the PWM signal. In an analog circuit, a comparator is used for comparing the control signal V_c to a sawtooth wave (or a triangular wave) V_{tri} . Therefore, it is ON when $V_c > V_{tri}$ and OFF when $V_c < V_{tri}$.

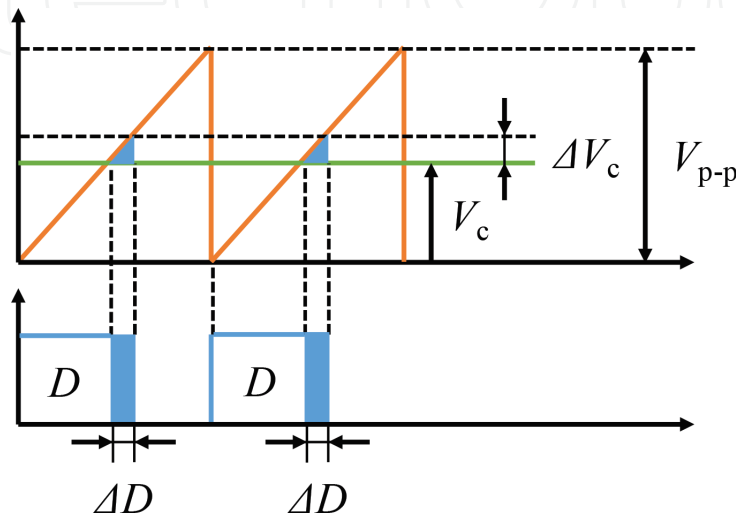


Figure 3.
PWM modulation F_m .

The ratio per switching cycle of this relationship is the duty ratio. When a small disturbance $\Delta V_c(s)$ occurs in the control voltage V_c , a small disturbance $\Delta D(s)$ is generated in the duty ratio D in the steady state. The relationship between these is equal to the slope of the sawtooth wave in one switching cycle. Accordingly, when the amplitude of the sawtooth wave is V_{p-p} , the transfer function of the PWM gain F_m is expressed by Eq. (5).

$$F_m = \frac{\Delta D(s)}{\Delta V_c(s)} = \frac{1}{V_{p-p}} \quad (5)$$

From Eq. (5), when the amplitude of the sawtooth wave is $V_{p-p} = 1$ V, the PWM gain F_m can be neglected.

2.3 Sensor gain: K_v and K_i

When current and voltage are used for feedback directly, the sensor gain can be neglected. However, when the voltage is high, it is necessary to lower it to the voltage value that can be provided to the controller. In addition, when inputting the current value to the controller, it is necessary to convert it into voltage. Therefore, when designing a control system, it is necessary to consider various sensor gains. In this chapter, the voltage gain is denoted by K_v and the current gain is denoted by K_i .

3. Conventional control methods for the DC-DC converter

In this section, voltage mode control (VMC) and current mode control (CMC) are compared to the power balance mode control (PBMC).

3.1 Voltage mode control (VMC)

Figure 4 shows the block diagram of the VMC. As shown, the control loop is configured to maintain a constant output voltage. The loop transfer function $G_{loop}(s)$ of the VMC is given in Eq. (6). This control system is the simplest feedback system.

$$G_{loop}(s) = G_{cv}(s) \cdot F_m \cdot G_{vd}(s) \cdot K_v \quad (6)$$

However, there is a long phase lag due to the second-order lag system $1/P(s)$ in the plant $G_{vd}(s)$. Furthermore, due to the RHP-zero, there is a phase delay of up to -270° at the plant $G_{vd}(s)$. Therefore, it is necessary to design a compensator for improving such a long phase delay.

In addition, there is a gain peak owing to the LC resonance. As a result, large overshoots or undershoots can occur in the inductor current and the output voltage following sudden changes such as load changes. In particular, the peak inductor

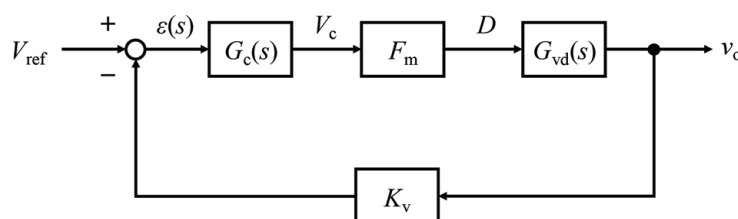


Figure 4.
Voltage mode control.

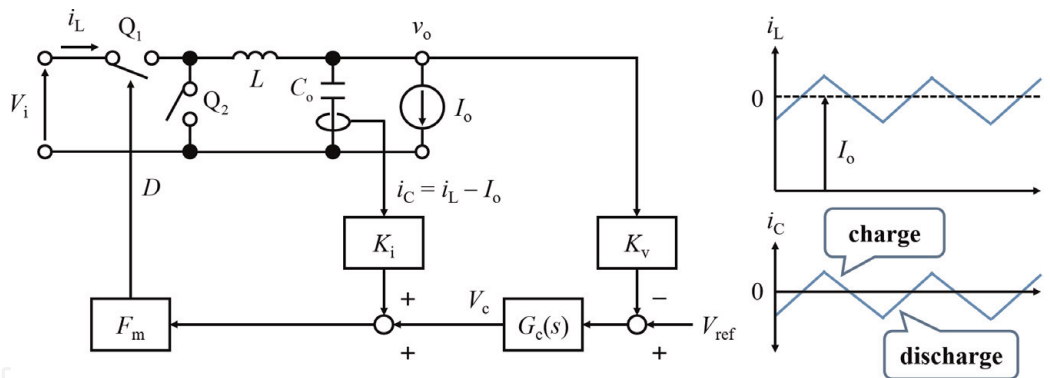


Figure 6.
 Buck-type DC-DC converter using sliding mode control.

Because the CMC also feeds back the inductor current, the duty ratio is finely adjusted. However, in the transient state, the inductor suppresses sudden changes in the current, and the system's responsiveness worsens.

On the other hand, when the charge/discharge current of the output capacitor is used as the feedforward input, the charge/discharge current in the transient state rapidly changes depending on the capacitor. As a result, the duty ratio can be changed faster than for the CMC. Furthermore, when shifting from the transient state to the steady state, the average charge/discharge current becomes zero, and the influence of the feedforward input automatically decreases. Therefore, the feedforward input gain automatically becomes minimal during the transient and in the steady state.

In addition, by appropriately designing the various sensor gains and compensators of this control system, it is possible to set an operation state called the sliding mode. It is known that the control system operating in this sliding mode is not affected by disturbances or plant fluctuations. Therefore, responsiveness and robustness can be improved by operating in sliding mode.

Although this output capacitor current can be detected directly, equivalent series resistance (ESR) and equivalent series inductance (ESL) increase owing to the addition of a shunt resistance and a current transformer, which affects the control system and output voltage. In addition, in digital control systems, analog-to-digital conversion cannot be performed precisely owing to an increase in the noise associated with charging/discharging. On the other hand, it is possible to derive the charge/discharge current of the output capacitor without directly detecting it, by appropriately detecting the output current and the inductor current and performing the calculation. However, as the inductor current of the boost-type DC-DC converter flows only to the output side during the OFF period, the output current differs from the inductor current.

Therefore, it is necessary to consider the control system corresponding to the step-up-type DC-DC converter considering output capacitor current detection and digital control. In the next section, we describe the PBMC with improved responsiveness and robustness for boost-type DC-DC converters.

4.2 Power balance mode control

Figure 7 shows the block diagram of the PBMC. First, various blocks are described.

- $G_{cv}(s)$: transfer function of voltage compensator
- K_{vo} : output voltage sensor gain

- K_{io} : output current sensor gain
- K_{vi} : input voltage sensor gain
- K_{ii} : input current (inductor current) sensor gain

In addition, $a, b, c, d,$ and e denote the correction coefficients. Further, the mathematical symbols \times and \div are the multiplier and the divider, respectively. As shown in **Figure 7**, these correction coefficients are applied to all output signals from various sensor gains. For simplicity, the correction coefficients $a, b, c,$ and d are the inverses of the sensor gain. Accordingly, the various correction coefficients are given in Eq. (8).

$$\begin{cases} a = 1/K_{vo} \\ b = 1/K_{io} \\ c = 1/K_{vi} \\ d = 1/K_{ii} \end{cases} \quad (8)$$

As a result, all output signals of the correction coefficients' block can be considered as the values for the power stage.

First, when the detected output voltage and output current are fed into the multiplier, the output is expressed by Eq. (9).

$$v_o \cdot K_{vo} \cdot a \cdot i_o \cdot K_{io} \cdot b \approx v_o \cdot i_o = P_o^* \quad (9)$$

Thus, the output power can be calculated. Next, when the calculated output power and the detected input voltage are provided to the divider, the output is expressed by Eq. (10).

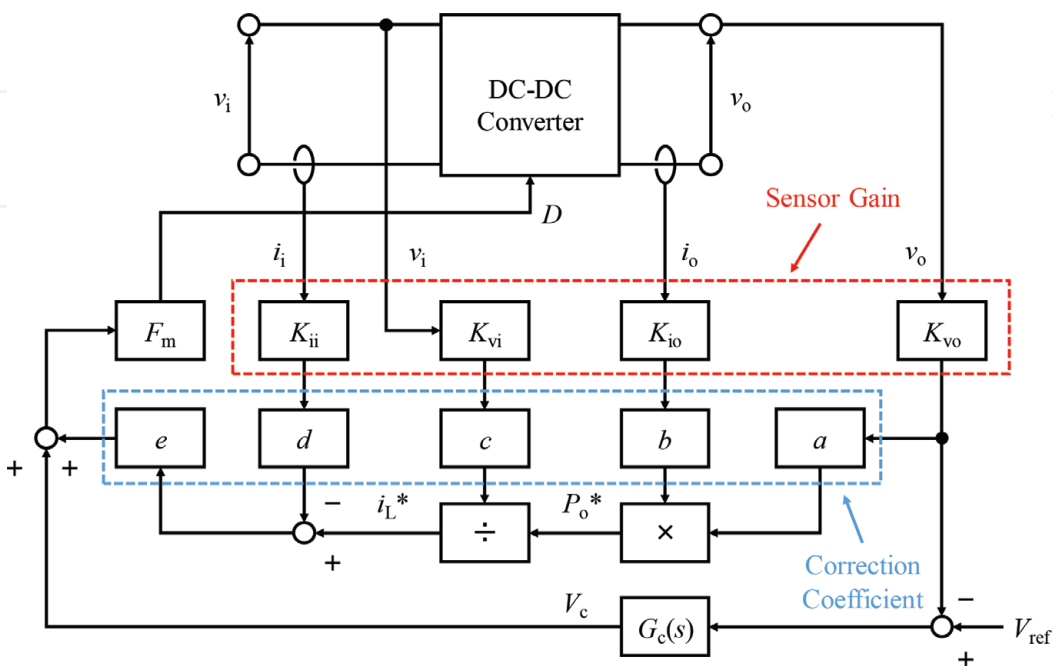


Figure 7.
Power balance mode control.

$$\frac{v_o \cdot K_{v_o} \cdot a \cdot i_o \cdot K_{i_o} \cdot b}{v_i \cdot K_{v_i} \cdot c} \approx \frac{v_o \cdot i_o}{v_i} = i_i^* = i_L^* \quad (10)$$

Thus, the input current can be calculated. Because the input current of the boost-type DC-DC converter is equivalent to the inductor current, it is denoted by i_L^* . Finally, the calculated inductor current is compared with the detected inductor current, and the final duty ratio is determined by adding the result of this comparison and the output of the voltage compensator. From the relationship between the calculated inductor current i_L^* and the detected inductor current i_L , the operation can be divided into the following three patterns. **Figure 8** shows the flowchart of the control methods.

4.2.1 Mode 1: $i_L^* > i_L$

In this mode, the calculated inductor current i_L^* is higher than the detected inductor current i_L . As an example, consider the case in which a shift to a heavy load occurs. Because the output current suddenly extracts electric charge from the output capacitor, the calculated output P_o^* power increases. On the other hand, as the input voltage corresponds to a DC voltage source such as a battery, the voltage does not fluctuate significantly even when the load fluctuates. Therefore, the calculated

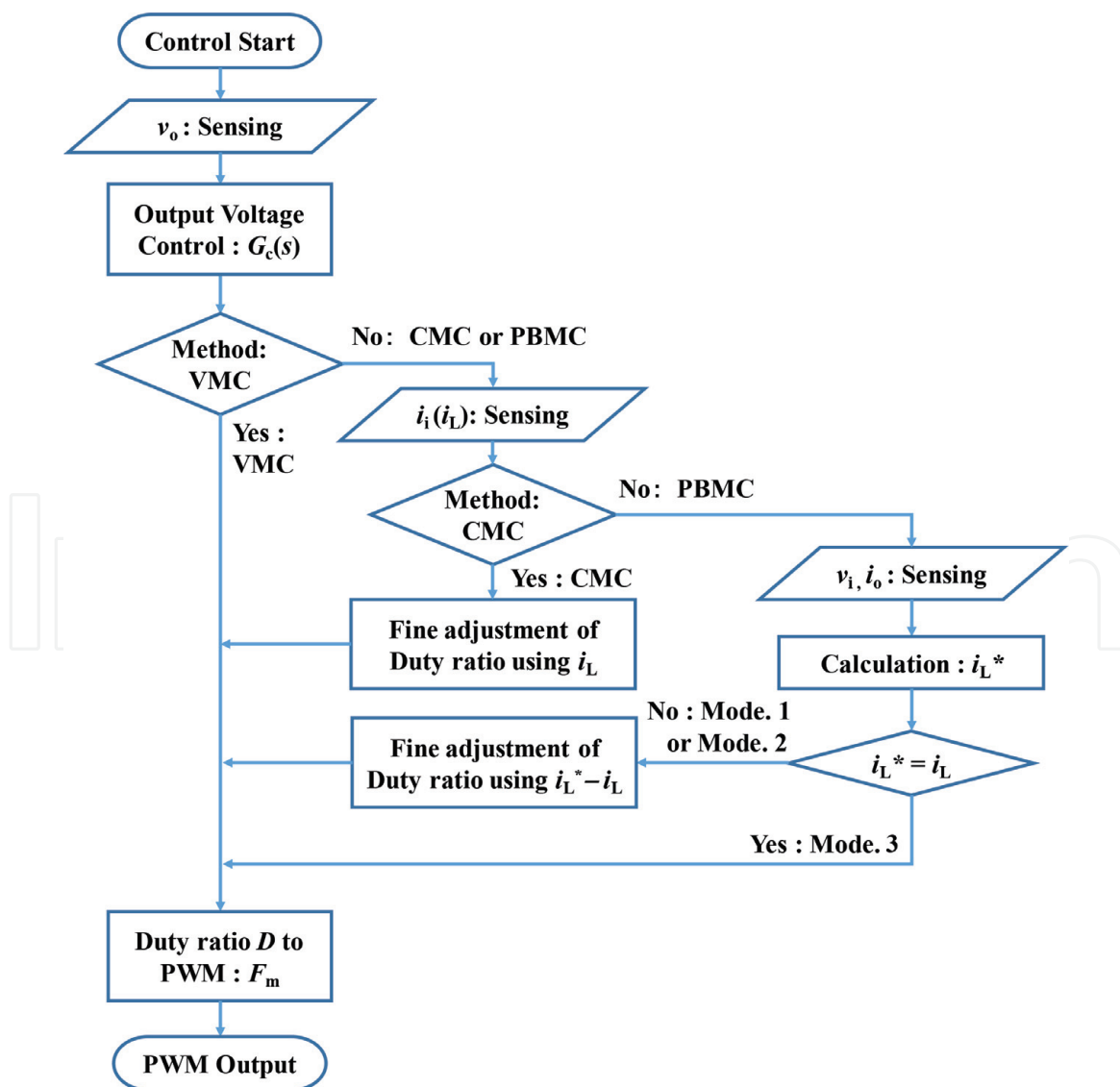


Figure 8.
 The flowchart of the control methods.

inductor current i_L^* increases according to the load. In contrast, the inductor current for detection increases. Therefore, until the input power becomes equal to the output power, the relationship of Eq. (11) holds.

$$i_L^* > i_L \quad (11)$$

As a result, the signal to be added to the output signal of the voltage compensator becomes positive and the duty ratio increases.

4.2.2 Mode 2: $i_L^* < i_L$

In this mode, the calculated inductor current i_L^* is lower than the detected inductor current i_L . An example would be the case in which a shift to a light load occurs. Because the output current suddenly extracts electric charge from the output capacitor, the calculated output P_o^* power decreases. On the other hand, as the input voltage corresponds to a DC voltage source such as a battery, the voltage does not fluctuate significantly even when the load fluctuates. Therefore, the calculated inductor current i_L^* decreases according to the load. In contrast, the inductor current for detection increases. Therefore, until the input power becomes equal to the output power, the relationship of Eq. (12) holds.

$$i_L^* < i_L \quad (12)$$

As a result, the signal to be added to the output signal of the voltage compensator becomes negative and the duty ratio decreases.

4.2.3 Mode 3: $i_L^* = i_L$

In this mode, the calculated inductor current is equal to the detected inductor current. This corresponds to a steady state, and because the input and output powers are ideally equal, the following relation holds:

$$i_L^* = i_L \quad (13)$$

As a result, as the signal to be added to the output signal of the voltage compensator becomes zero, the duty ratio does not fluctuate.

These conditions are summarized in Eq. (14).

$$\begin{cases} i_L^* > i_L & \text{if } P_o > P_i \\ i_L^* < i_L & \text{if } P_o < P_i \\ i_L^* = i_L & \text{otherwise } (P_o = P_i) \end{cases} \quad (14)$$

To sum up, the PBMC is a control method that always compares the input power and the output power and compensates for the difference if there is one. In the next sections, operation verification studies for the different control methods are reported.

5. Control design and simulation verification

5.1 Control design

In this study, a comparative verification of the different control systems was performed using circuit simulations. **Table 1** shows the circuit constants of the

Description	Symbol	Value
Inductor current (100 W design)	I_L	8.33 A
Output voltage	V_o	48 V
Output power	P_o	100/200 W
Switching frequency	f_s	100 kHz
Inductance (100 W design)	L	36 μ H
Output capacitance (100 W design)	C_o	500 μ H
Equivalent series resistance (ESR) of C_o	r_C	58.5 m Ω
DC resistance of L (DCR)	r_L	20 m Ω
Resistance of drain to source (ON) of Q_1	r_Q	58 m Ω
Forward resistance of Q_1 (diode: D)	r_D	130 m Ω

Table 1.
 Circuit parameters and specifications.

single-phase boost-type DC-DC converter, which is the analysis circuit. The control systems were constructed using these circuit parameters.

To provide a reference for the responses of these control systems, the gain cross-over frequencies of the loop transfer functions for the different control methods were designed to be equal. In addition, the voltage compensator for the PBMC used the same 2-pole-1-zero (type-2) compensator as the current mode control.

5.1.1 Voltage mode control (VMC)

The transfer function of the VMC includes second-order lag systems, as expressed by Eq. (4). In addition, the phase lags by 180° or more, owing to the RHP-zero. To improve the phase delay and to stabilize the operation of the control system, a 3-pole-2-zero (type-3) compensator was used. The transfer function of this 3-pole-2-zero compensator is given in Eq. (15).

$$G_c(s) = \frac{\omega_i}{s} \cdot \frac{\left(1 + \frac{s}{\omega_{z1}}\right) \left(1 + \frac{s}{\omega_{z2}}\right)}{\left(1 + \frac{s}{\omega_{p1}}\right) \left(1 + \frac{s}{\omega_{p2}}\right)} \quad (15)$$

5.1.2 Current mode control (CMC)

A secondary delay system was included in both $G_{vd}(s)$ and $G_{vd}(s)$ in the loop transfer function of the CMC. However, the current control loop is in the inner loop, and the second-order lag system is approximately canceled out. Therefore, the phase delay became smoother, when compared with VMC, and the resonance peak did not appear. Therefore, the CMC used a 2-pole-1-zero (type-2) compensator. The transfer function of the 2-pole-1-zero compensator is given in Eq. (16).

$$G_c(s) = \frac{\omega_i}{s} \cdot \frac{\left(1 + \frac{s}{\omega_z}\right)}{\left(1 + \frac{s}{\omega_p}\right)} \quad (16)$$

where ω_i , integral frequency; ω_z , zero point frequency (ω_z and ω_{z1} : first point, ω_{z2} : second point); ω_p , pole frequency (ω_p and ω_{p1} : first point, ω_{p2} : second point).

5.1.3 Power balance mode control (PBMC)

In the PBMC, the difference between the calculated inductor current i_L^* and the detected inductor current i_L is added to the output signal of the voltage compensator. The responsiveness of the output voltage is determined by the crossover frequency in the open loop transfer function. Therefore, the change in the inductor current's reference value (calculated inductor current i_L^*) is much slower than the change in the detected inductor current i_L . Therefore, if the reference value of the inductor current is regarded approximately as the DC value in the steady state, it is almost equivalent to the configuration of the CMC.

Therefore, the voltage compensator used a 2-pole-1-zero compensator similar to the CMC. In our simulations, for simplicity, the values of the correction coefficients a , b , c , and d were set to 1. However, for the CMC, e was set to the CMC's current sensor gain ($e = K_i = 0.08$). In addition, by setting the various sensor gains according to Eq. (17), calculation of the power balance control loop can be easily dealt with.

$$\begin{cases} K_{vo} = 1/V_o \\ K_{io} = 1/I_o \\ K_{vi} = 1/V_i \\ K_{ii} = 1/I_i \end{cases} \quad (17)$$

Various parameters represented by capital letters on the right side of Eq. (17) are design values. As a result, the input/output voltage/current/power parameters were all 1 by design.

5.2 Comparative verification using circuit simulation

In this section, a comparative verification of each control system using circuit simulation is described. For the simulation, a circuit simulator PSIM manufactured by Powersim Corporation is used. Configure the configuration of the power stage and control stage using PSIM. The circuit constants of the power stage are shown in **Table 1**, and the parameters of the voltage compensator of the control stage are shown in **Table 2** described later. In addition, each sensor gain and correction constants are as in Section 5.1.3.

Table 2 shows the compensators' parameters for the different control methods. In addition, the gain crossover frequency of the loop transfer function was $\omega_c = 6283.19$ rad/s ($f_c = 1.0$ kHz). The extent of the fluctuation and the settling time of the output voltage and the inductor current during the transient state of the load and the input voltage were compared. The load transients were a step-up load transient that fluctuated from 100 to 200 W and a step-down load transient that fluctuated from 200 to 100 W. In addition, the input voltage transients were a step-up input voltage transient that fluctuated from 12 to 24 V and a step-down input voltage transient that fluctuated from 24 V to 12 V. In the simulations, the ripple component was large and it was difficult to identify the different components.

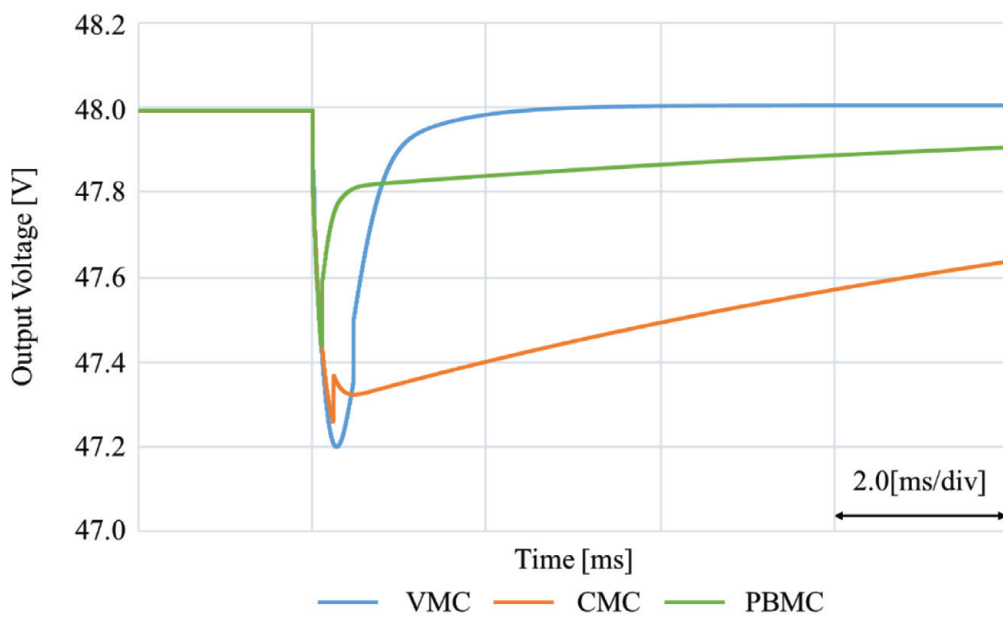
$G_c(s)$	ω_i (rad/s)	ω_{z1} (ω_z) (rad/s)	ω_{z2} (rad/s)	ω_{p1} (ω_p) (rad/s)	ω_{p2} (rad/s)
VMC	35.3	1.86×10^3	1.86×10^3	4.00×10^4	3.42×10^4
CMC	105.0	86.8	–	3.42×10^4	–
PBMC					

Table 2.
Compensator $G_c(s)$ parameters for different control methods.

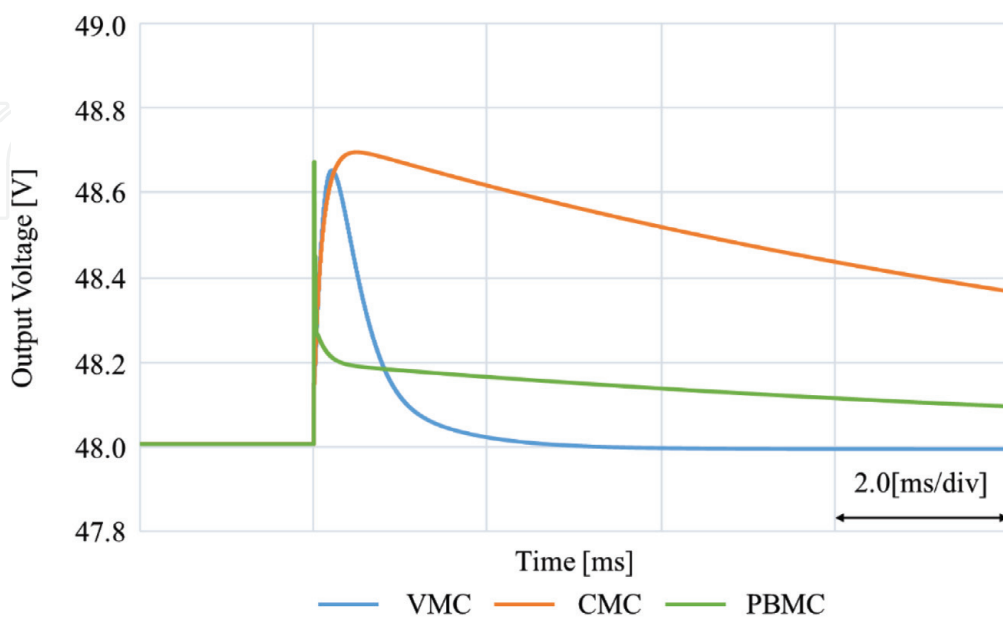
Therefore, the sampling frequency was reduced and a low-pass filter (LPF) was used. In addition, the settling time of the output voltage in the step response was set to the time required for reaching ± 0.2 V (approximately $\pm 1\%$) from the steady value of 48 V.

5.2.1 Output voltage response for load transients

Figure 9 shows the output voltage during load transient in each control method. Compared with CMC, over/undershoot of output voltage is small and settling time is short in PBMC. In particular, the settling time of the output voltage of the PBMC is very short compared with other control methods. Therefore, the PBMC can instantaneously respond to load fluctuations.



(a)



(b)

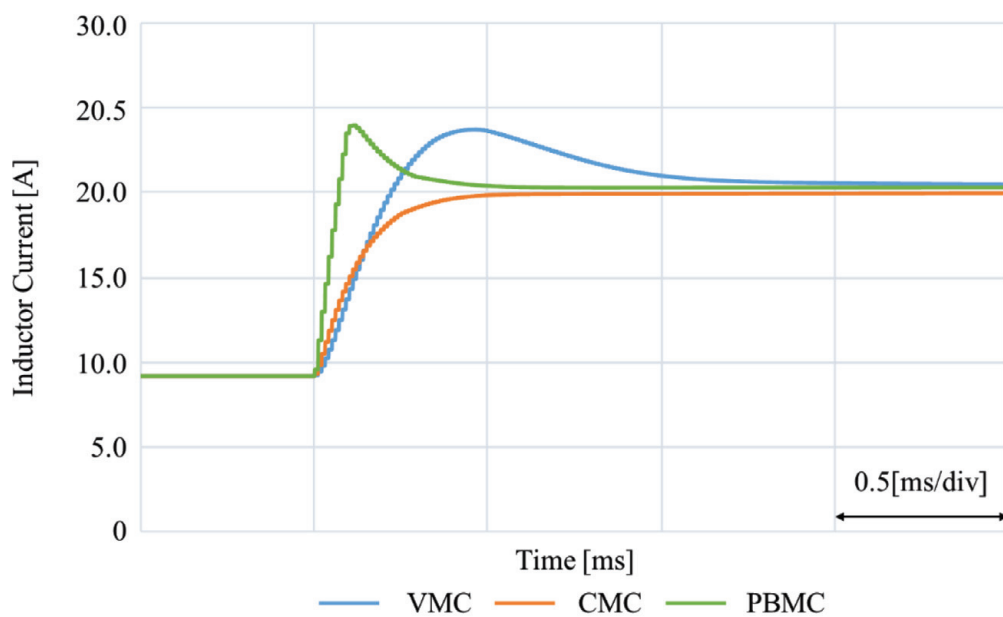
Figure 9. Output voltage responses for load transients. (a) Step-up load transient and (b) step-down load transient.

5.2.2 Inductor current response for load transients

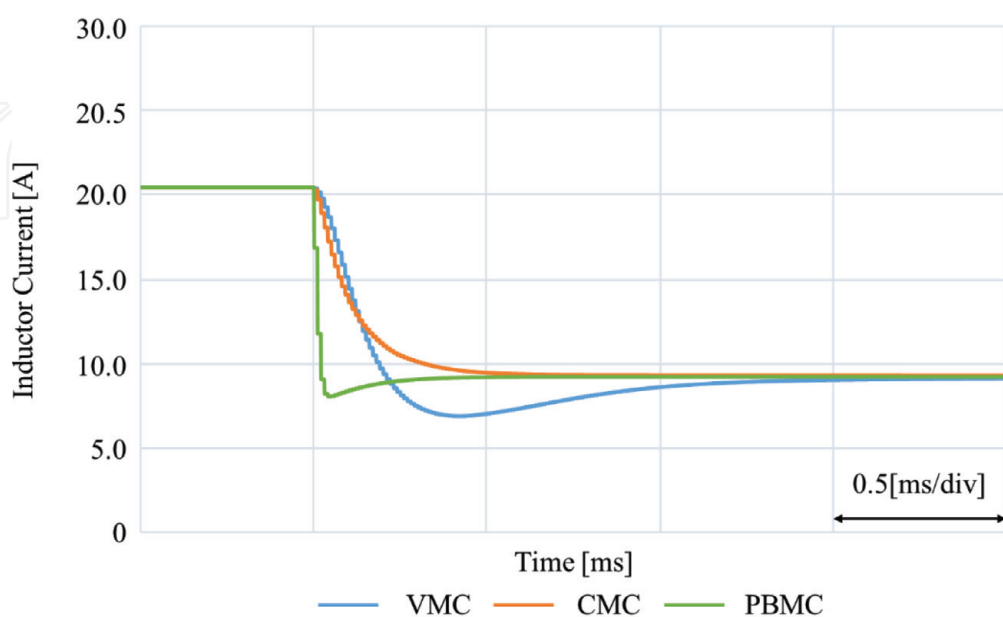
Figure 10 shows the inductor current during the load transient, for the different control methods. From **Figure 10**, the rise/fall time of the inductor current of the PBMC is very short compared with that of the other control methods. Because the rise/fall time of the inductor current of the PBMC is very short, the settling time of the output voltage becomes short. Although over/undershoots of the inductor current also appear in the PBMC, the outcome can be improved by appropriately setting the correction coefficient E .

5.2.3 Output voltage response for input voltage transients

Figure 11 shows the output voltage during the input voltage transient, for the different control methods. Compared with the other control methods, the over/

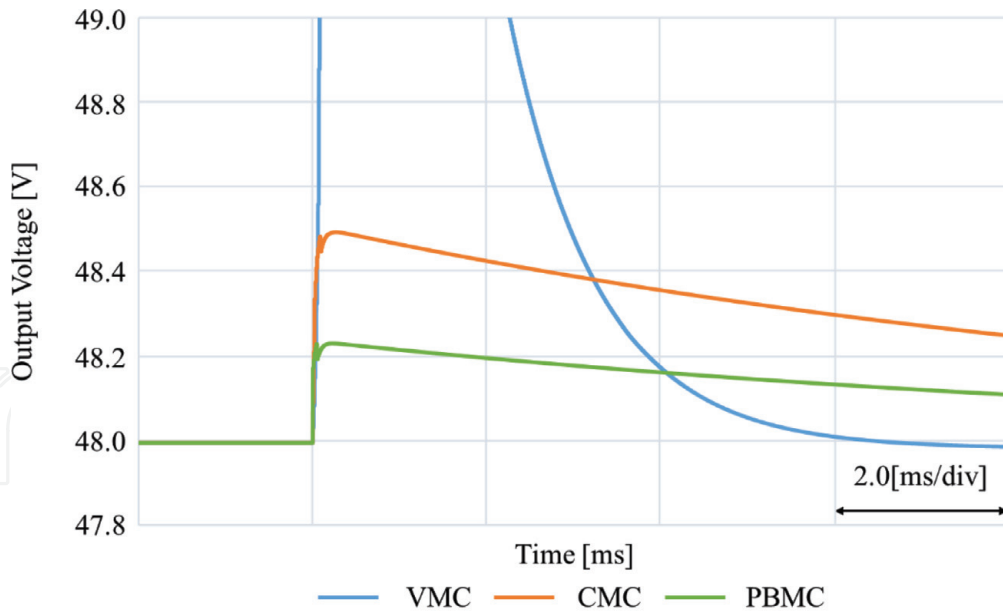


(a)

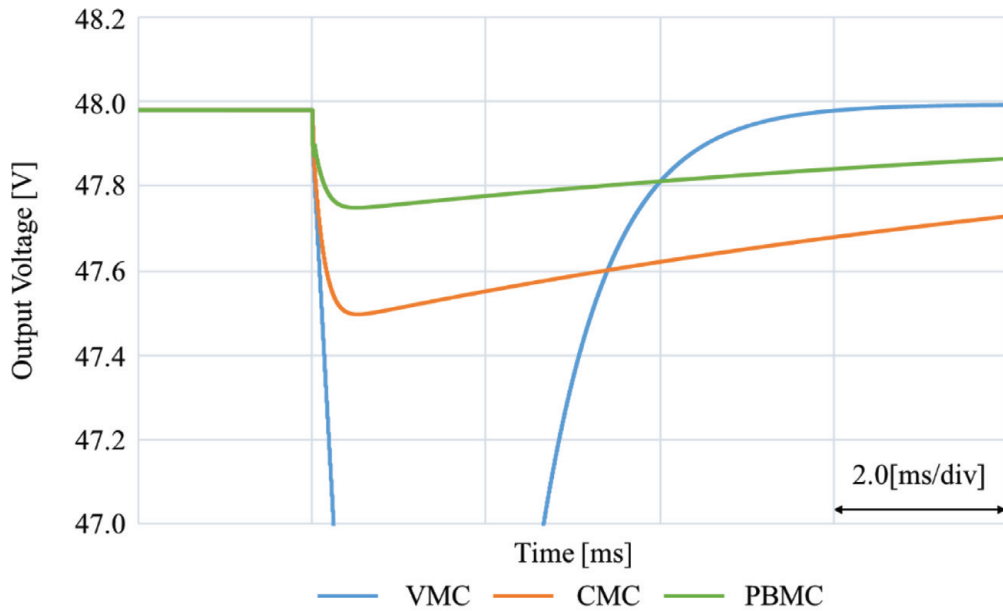


(b)

Figure 10. Inductor current responses for load transients. (a) Step-up load transient and (b) step-down load transient.



(a)



(b)

Figure 11. Inductor current responses for input voltage transients. (a) Step-up input voltage transient and (b) step-down input voltage transient.

undershoot of output voltage is smaller and the settling time is shorter for the PBMC method. Therefore, a system with PBMC can instantaneously respond to input voltage fluctuations.

5.2.4 Inductor current response for input voltage transients

Figure 12 shows the inductor current during the input voltage transient, for the different control methods. From **Figure 12**, the rise/fall time of the inductor current for the PBMC method is much shorter compared with that of the other control methods. Because the rise/fall time of the inductor current for the PBMC method is very short, the settling time of the output voltage is short.

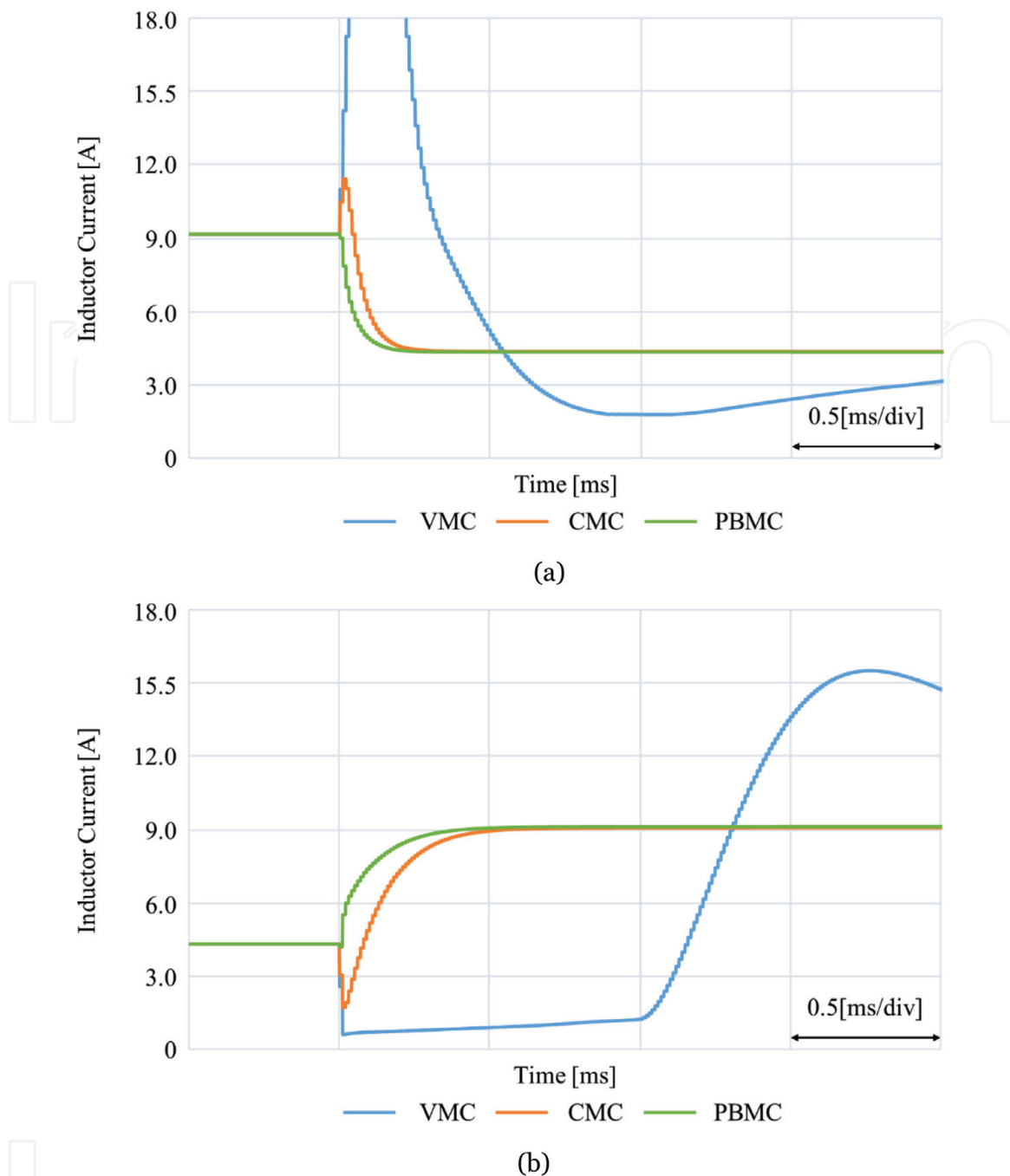


Figure 12. Inductor current responses for input voltage transients. (a) Step-up input voltage transient and (b) step-down input voltage transient.

5.2.5 Comparative verification of simulation results

The simulation results for the different control methods are compared below. **Table 3** lists the simulation results for the load transient response, and **Table 4** shows the simulation results for the input voltage transient response. The most efficient results are shown by *, while the least efficient ones are shown by **. From these tables, it is evident that the PBMC method yields the most efficient results in terms of almost all metrics, when compared with the other control systems. The effectiveness of the PBMC method is confirmed across all simulation results.

VMC method has only output components. Therefore, it is impossible to promptly respond to input fluctuations. Therefore, the overshoot and undershoot in the input voltage fluctuation are much larger than the other two control methods.

Target value V_o : 48 V	Step-up transient		Step-down transient	
	Undershoot (mV)	Settling time (ms)	Overshoot (mV)	Settling time (ms)
VMC	795.1**	0.77	646.7*	0.78
CMC	735.2	15.10**	690.6**	14.96**
PBMC	554.6*	0.40*	667.1	0.29*

Table 3.
 Simulation results for the load transient response.

Target value V_o : 48 V	Step-up transient		Step-down transient	
	Overshoot (mV)	Settling time (ms)	Undershoot (mV)	Settling time (ms)
VMC	4531.9**	3.86	4048.5**	3.96
CMC	498.7	10.18**	484.9	11.69**
PBMC	235.5*	1.61*	231.8*	3.30*

Table 4.
 Simulation results for the input voltage transient response.

CMC method has input and output components one by one. However, even during transient, the settling time is long because it is always approximated to the first-order lag system.

PBMC method has all components of input and output. Therefore, it is thought that it be able to respond quickly to input/output fluctuations.

6. Conclusion

This chapter described fast-response and highly robust PBMC for boost-type DC-DC converters. PBMC uses control to compensate for the difference between input power and output power for the inner loop. Performances of the PBMC method and conventional control methods were compared and verified using circuit simulations. As a result, the PBMC method yielded the best results on all performance metrics. This confirms the effectiveness of PBMC.

Author details

Taichi Kawakami
 Department of Technological Systems, Osaka Prefecture University College of Technology (OPUCT), Osaka, Japan

*Address all correspondence to: t.kawakami@osaka-pct.ac.jp

IntechOpen

© 2018 The Author(s). Licensee IntechOpen. This chapter is distributed under the terms of the Creative Commons Attribution License (<http://creativecommons.org/licenses/by/3.0>), which permits unrestricted use, distribution, and reproduction in any medium, provided the original work is properly cited. 

References

- [1] Erickson RW, Maksimovic D. Fundamentals of Power Electronics. 2nd ed. Berlin: Springer; 2001. pp. 331-375. DOI: 10.1007/b100747. Ch 9
- [2] Figueres E, Garcera G, Benavent JM, Pascual M, Martinez JA. Adaptive two-loop voltage-mode control of DC-DC switching converters. IEEE Transactions on Industrial Electronics. 2006;**53**(1): 239-253. DOI: 10.1109/TIE.2005.862254
- [3] Choi B. Pulsewidth Modulated DC-To-DC Power Conversion: Circuits, Dynamics, and Control Designs. USA: Wiley; 2013. pp. 465-557. DOI: 10.1002/9781118772188. Ch 10
- [4] Bryant B, Kazimierczuk MK. Voltage loop of boost PWM DC-DC converters with peak current-mode control. IEEE Transactions on Power Electronics. 2006;**53**(1):99-105. DOI: 10.1109/TCSI.2005.854611
- [5] Tan SC, Lai YM, Tse CK, Cheung MKH. Adaptive feedforward and feedback control schemes for sliding mode controlled power converters. IEEE Transactions on Power Electronics. 2006;**21**(1):182-192. DOI: 10.1109/TPEL.2005.861191
- [6] Tan SC, Lai YM, Tse CK. A unified approach to the design of PWM-based sliding-mode voltage controllers for basic DC-DC converters in continuous conduction mode. IEEE Transactions on Circuits and Systems I: Regular Papers. 2006;**53**(8):1816-1827. DOI: 10.1109/TCSI.2006.879052
- [7] Tan SC, Lai YM, Tse CK. General design issues of sliding-mode controllers in DC-DC converters. IEEE Transactions on Industrial Electronics. 2008;**55**(3):1160-1174. DOI: 10.1109/TIE.2007.909058
- [8] Tan SC, Lai YM, Tse CK. Sliding Mode Control of Switching Power Converters: Techniques and Implementation. USA: CRC; 2012. pp. 105-129. DOI: 10.1109/MIE.2012.2207832. Ch 6
- [9] Ling R, Maksimovic D, Leyva R. Second-order sliding-mode controlled synchronous Buck DC-DC converter. IEEE Transactions on Power Electronics. 2016;**31**(3):2539-2549. DOI: 10.1109/TPEL.2015.2431193
- [10] Kawakami T, Harada T, Yamamoto M, Umetani K. Proposal for the new control method having high Resiponsiveness and high robustness for the boost-type DC-DC converter. IEEJ Transactions on Electronics, Information and Systems. 2018;**138**(4): 395-404. DOI: 10.1541/ieejeiss.138.395
- [11] Choi B. Pulsewidth Modulated DC-To-DC Power Conversion: Circuits, Dynamics, and Control Designs. USA: Wiley; 2013. pp. 199-244. DOI: 10.1002/9781118772188. Ch 5
- [12] Erickson RW, Maksimovic D. Fundamentals of Power Electronics. 2nd ed. Berlin: Springer; 2001. pp. 187-263. DOI: 10.1007/b100747. Ch 7
- [13] Smithson SC, Williamson SS. A unified state-space model of constant-frequency current-mode-controlled power converters in continuous conduction mode. IEEE Transactions on Industrial Electronics. 2015;**62**(7): 4515-4524. DOI: 10.1109/TIE.2015.2412514